IEEE Access
Multidisciplinary | Rapid Review | Open Access Journal

Received September 18, 2020, accepted October 1, 2020, date of publication October 6, 2020, date of current version October 22, 2020.

Digital Object Identifier 10.1109/ACCESS.2020.3028845

Integral Super Twisting Sliding Mode Based Sensorless Predictive Torque Control of Induction Motor

IRFAN SAMI[1], SHAFAAT ULLAH[2], ABDUL BASIT[2], NASIM ULLAH[3], AND JONG-SUK RO[1]

[1]School of Electrical and Electronics Engineering, Chung-Ang University, Seoul 06974, South Korea
[2]COMSATS University Islamabad, Abbottabad Campus, Abbottabad 22060, Pakistan
[3]College of Engineering, Department of Electrical Engineering, Taif University, Ta'if 26571, Saudi Arabia

Corresponding author: Jong-Suk Ro (jongsukro@gmail.com)

This work was supported in part by the Basic Science Research Program through the National Research Foundation of Korea funded by the Ministry of Education under Grant 2016R1D1A1B01008058; and in part by the Human Resources Development of the Korea Institute of Energy Technology Evaluation and Planning (KETEP) Grant funded by the Korea government Ministry of Trade, Industry and Energy, under Grant 20204030200090.

ABSTRACT In the direct torque control (DTC) of induction motor (IM) drive systems utilizing model predictive torque control (MPTC) in the inner loop and classical proportional integral (PI) control in the outer loop is prone to weaknesses, such as uncertainties, external disturbances, parameter variations, and nonlinear dynamics. A high-performance control system for speed and torque is required to guarantee a smooth and robust control architecture that can withstand such unpredictable effects. In this study, we propose an integral super twisting sliding mode control (ISTSMC) to address the shortcomings of the classical PI used in the outer loop of DTC drive systems. A sliding mode speed observer is also designed and utilized to overcome problems associated with mechanical sensors. The robustness of the proposed control strategy and fast dynamic speed response are compared favorably with a benchmark PI controller and conventional sliding mode control (SMC). The ability of the proposed system to regulate both speed and torque was evaluated through simulations, under various fault perturbations, parameter variations, and load disturbances, conducted in MATLAB/ Simulink. Various performance indices were used to demonstrate the superior performance of the proposed strategy compared to a benchmark PI system and conventional SMC-based MPTC approaches.

INDEX TERMS Direct torque control (DTC), induction motor (IM), model predictive torque control (MPTC), sliding mode control (SMC), sliding mode observer (SMO), super twisting control (STC).

I. INTRODUCTION

Induction machines are widely used in industrial applications, such as conveyor belts and electric motors, because they are relatively robust, cost-effective, and simple in design. With the progressive development of electric vehicles and renewable wind energy utilizationnowadays, induction motor (IM) control design is increasingly important in both research and industry, as the complex, nonlinear models of these motors make precise control difficult [1], [2]. Direct torque control (DTC) schemes, also known as bang-band controllers, were initially proposed for the IM by Takahashi and Noguchi in 1986 [3], and by Depenbrock in 1988 [4], and are used extensively for high-performance AC drives for their simple decoupled topology. Two cascaded loops are used in these systems: (1) an inner loop, which generates a reference stator flux and torque, and (2) an outer loop, which is implemented through lookup-table-based hysteresis control using the references generated by the inner loop. The DTC is one of the most robust control technique owing to its insensitivity to control parameters [5]. However, conventional DTC operation is prone to problems, such as unwanted noise, high torque ripples, and extra losses resulting from the hysteresis band application in the inner loop [6], [7]. Increasing the hysteresis band decreases the inverter switching frequency, leading to increased torque ripples, while decreasing the hysteresis band causes the switching frequency to increase, which subsequently increases the inverter losses [8].

Several techniques have been proposed to overcome the stated DTC drawbacks, such as artificial intelligence and

The associate editor coordinating the review of this manuscript and approving it for publication was Zheng Chen.

extended switching tables [9], [10]. Among these emerging control strategies, model predictive torque control (MPTC) achieved by introducing model predictive control (MPC) in the inner loop is the most attractive for both industrial and academic communities, owing to its quick dynamic response, intuitive concepts, multi-variable control, low torque and flux ripples, and nonlinear capabilities [11]–[13] for the inner loop. In high-performance AC motor drives, MPTC has been considered as an alternative to both field oriented control (FOC) and DTC [14], and it meets all modern control system requirements: (1) digital control platforms, (2) use of plant models, and (3) consideration of system constraints and limitations [15].

The collection of speed information is a critical component of the IM speed and torque control in MPTC strategies [16]. Typically, speed is measured through mechanical sensors and then fed back to the summing junction in the inner loop, to generate the reference torque. Conventional mechanical sensors suffer from wear and tear over time as it is continually used, and several techniques have been introduced to address this problem, including open-loop estimators, full-order observers, reduced-order observers, adaptive reference models, Kalman filters, and neural networks [17].

For sensorless schemes, a technique known as sliding mode (SM) is an attractive performance-enhancing choice, because of its rapid and dynamic robustness against external turbulences, incorrect parameters, and noise [17]. Sliding mode observers (SMOs) have been previously proposed in the literature for sensorless control of motor drives. An observer was designed in [18] to estimate system disturbances for improved control of permanent magnet synchronous motors (PMSMs). Ammar *et al.* [19] used an SM approach to design dual SMOs to estimate load torque, speed, and flux for space-vector-modulation-based DTC of the IMs. Wang *et al.* [20] proposed an SMO for linear IMs to estimate their online resistance, flux, and speed, while Kubota and Matsuse [21] theoretically showed that rotor resistance and speed can only be estimated simultaneously when the magnitude of the flux varies periodically, and not on a permanent basis. Considering these drawbacks, increasing the robustness of estimators and observers by simultaneously estimating the rotor speed and the IM parameters can be a very complex challenge. However, it is possible to achieve greater robustness, even in the presence of parameter variations, by appropriately selecting the observer feedback gains [22], [23]. For example, an SM-based rotor resistance and speed observer was presented in [24] for achieving indirect FOC of the IMs. The proposed algorithm used estimated stator currents to observe speed through continuous-time SM functions. Such SMOs have recently been applied to estimate the position, flux, current, and speed errors of switched reluctance motors [25]. Ma and Zhang [26] used an SM approach to detect the direction of rotation of PMSMs, using actual stator current as the error trajectory. Alternatively, in this study we propose an SMO for estimating the IM speed without using an online estimation of the IM parameters. First, a current observer is designed using the first-order SM. Then, the rotor speed is estimated based on the Lyapunov stability theory. The sensorless PI-based MPTC strategy presented herein is further enhanced by introducing robust controllers for both speed and current regulation.

The PI controller is one of the commonly implemented controllers in the outer loop for speed and torque regulation. Rodriguez *et al.* proposed a predictive controller formed by using a PI controller in the outer loop [27], while Miranda *et al.* presented a predictive IM torque control technique that utilizes the state-space model, along with the PI controller, to calculate a reference torque [28]. Additionally, Habibullah *et al.* proposed a technique based purely on finite-state model predictive control (MPC), using a PI control scheme [29], and Ahmad *et al.* developed a control scheme based on a state-tracking cost index, which utilized PI control in the inner loop [30].

Sliding mode control (SMC) is ultimately more robust and disturbance-resistant than PI control [31], [32], and the hardware and software implementation are quite simple. Notably, an SM-based MPTC strategy has been proposed by Sami *et al.* [33]. In general, SMC methods offer good dynamic response and robustness for the IM drives. However, they have rarely been applied for speed and torque control, due to inherent chattering problems, which are quite common in the first-order SMCs [34]. The performance of the first-order SMCs has been enhanced by various techniques, but the most common is approximating the discontinuous ''signum'' function by the continuous ''saturation'' or ''sigmoid'' function, which minimizes chattering [35]. While effective, this technique limits the control scheme performance under disturbances and fault perturbations, as the sliding system trajectory does not converge precisely to the sliding surface.

Adaptive SMC techniques have recently been proposed to adapt to reduced gain, with respect to faults and disturbances, which reduced chattering. An adaptive first-order SMC for electro-pneumatic actuators was proposed in [36], and other developing enhancement techniques, summarized in Fig. 1, that includes design of various reaching law approaches, sliding surfaces, higher order SMCs, and composite SMCs. Numerous SMC variants have been proposed in to improve its performance. Recently, a fast and non-singular fast terminal SMC (NFTSM) [37], followed by adaptive time-delay control with NFTSM has been proposed in [38] for cable driven manipulators. Another variant of SMC has been proposed in [39], [40] using fractional order terminal SMC for cable driven manipulators and robots.

Higher-order SMCs are derived from the generalization of the first-order SMCs. Instead of using only the first derivative of a sliding surface, this technique uses higher-order derivatives and provides extreme robustness and reduced chattering, making it viable for electric drives [41].

Currently, a super twisting sliding mode control (STSMC) technique has attracted significant attention, particularly for systems where the control law appears in the first

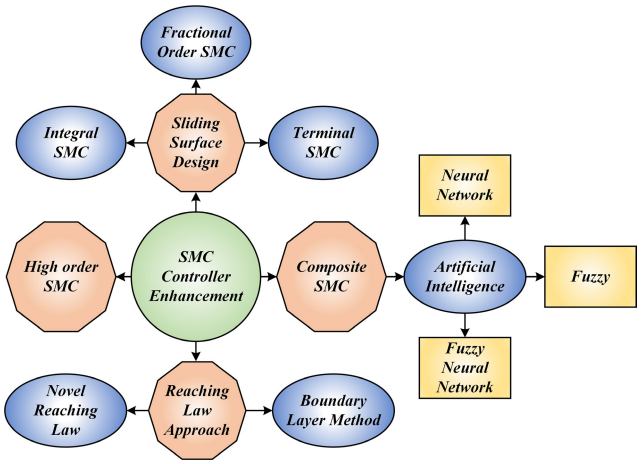

FIGURE 1. Enhancements made in SMCs throughout the field [31].

derivative of the sliding variable. The primary advantages of STSMC include [42]: (1) Compensation for Lipschitz perturbations/uncertainties, (2) only information about sliding variable, S, is required, (3) finite-time convergence to the origin for both S and the surface derivative, $\dot{S}$, are simultaneously provided, and (4) chattering by continuous control signals.

Li *et al.* adopted an SMO and STSMC [43] to reduce chattering and sensor problems in a vector control system for permanent magnet linear motors. Additionally, a real-time STSMC was proposed in [44] to control rotor flux linkages and mechanical velocity for squirrel-cage IMs, and they also proposed a first-order SMO to estimate the flux and load torque. In [45], various second-order SMC techniques, which were specially designed to optimize power efficiency, were adopted and practically implemented for wind energy conversion systems. Furthermore, in [46], [47], a super twisting technique played a key role in improving the performance of a fuel cell control system.

Considering the previous studies, we propose an integral super twisting SMC (ISTSMC) technique, which combines the attributes of both the STSMC and integral SMC schemes to eliminate chattering and improve the robustness and convergence of the IM torque and speed. The performance of the proposed SMO-based ISTSMC-MPTC scheme has been evaluated through extensive simulations conducted in MATLAB/Simulink. The performance and accuracy of the proposed strategy was also validated by various performance indices. The main contributions of this paper are as follows:

- The SMC scheme is enhanced by using high-order SMCs in the outer loop of the IM MPTC drive system. An ISTSMC is proposed to overcome the shortcomings of the first-order SMC schemes incorporating the advantages of STSMC PI-based surfaces to further stabilize the control scheme against external disturbances and fault perturbations.
- The disadvantages of mechanical sensors are eliminated by designing an SMO design using the IM terminal quantities.

The rest of the paper is organized as follows: Section II describes the IM mathematical model in an asynchronously revolving reference frame; Section III presents the ISTSMC design for the IM; sliding mode speed observer design is presented in Section IV; performance validation of the proposed strategy, carried out in MATLAB/Simulink, is provided in Section V; and finally the conclusions are discussed in Section VI.

II. INDUCTION MOTOR MODELING

The IM mathematical modeling described herein will be used to design the proposed ISTSMC-based sensorless MPTC approach. The assumptions made in the modeling of the IM are: (1) the stator winding should be distributed such that it produces sinusoidal magneto motive force (MMF) in uniform air gaps, (2) a squirrel-cage type rotor is used, and (3) various losses including hysteresis, eddy currents, and magnetic saturation, are negligible. The mathematical model of the IM in a stationary reference ($\alpha\beta$) frame, with stator currents and rotor flux, are described using the following equations [44]:

$$\begin{cases} \dfrac{d}{dt}i_\alpha = -\left(\dfrac{L_m^2\alpha_r + L_r R_s}{\varepsilon L_m}\right) i_\alpha + p\omega_r\varphi_\beta + \dfrac{L_r}{L_m}v_{s\alpha} \\ \quad +\alpha_r\varphi_\alpha \\ \dfrac{d}{dt}i_\beta = -\left(\dfrac{L_m^2\alpha_r + L_r R_s}{\varepsilon L_m}\right) i_\beta - p\omega_r\varphi_\alpha + \dfrac{L_r}{L_m}v_{s\beta} \\ \quad +\alpha_r\varphi_\beta \end{cases} \tag{1}$$

$$\begin{cases} \dfrac{d}{dt}\varphi_\alpha = L_m\alpha_r i_\alpha - p\omega_r\varphi_\beta - \alpha_r\varphi_\alpha \\ \dfrac{d}{dt}\varphi_\beta = L_m\alpha_r i_\beta + p\omega_r\varphi_\alpha - \alpha_r\varphi_\beta \end{cases} \tag{2}$$

$$\begin{cases} T_{em} = \dfrac{3}{2}p\,\mathrm{Im}\left\{\varphi_\alpha i_\beta - \varphi_\beta i_\alpha\right\} \\ \dot{\omega}_r = bT_{em} - a\omega_r - f \end{cases} \tag{3}$$

where i_α, i_β are the stator ($\alpha\beta$) currents, L_s, L_r are the inductances of the stator and rotor, respectively, L_m is the magnetizing inductance of the stator, R_s, R_r are the resistances of the stator and rotor, respectively, p is the number of pole pairs, ω_r is the rotor speed, φ_α, φ_β are the rotor ($\alpha\beta$) fluxes, respectively, $v_{s\alpha}$, $v_{s\beta}$ are the stator ($\alpha\beta$) voltages, respectively, T_{em} is the electromagnetic torque, f is the viscous friction coefficient, $b = 1/J$, where J is the moment of inertia, $a = f/J$, $f = \frac{T_L}{J}$, where T_L is the load torque, $\alpha_r = \frac{R_r}{L_r}$, and $\varepsilon = \frac{L_s \times L_r}{L_m} - L_m$.

A. MATHEMATICAL MODEL OF TWO-LEVEL VOLTAGE SOURCE INVERTER (2L-VSI)

In this study, a two-level voltage source inverter (2L-VSI) is used to feed the IM, as shown in Fig. 2. Each output leg has only two complementary controllable power semiconductor switches, therefore, the topology has eight possible switching states. The seven different voltages produced by the eight

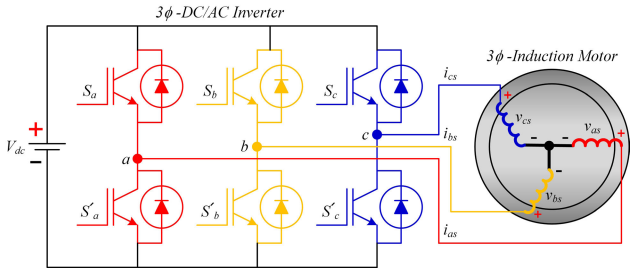

FIGURE 2. Illustration of the 2L-VSI circuit.

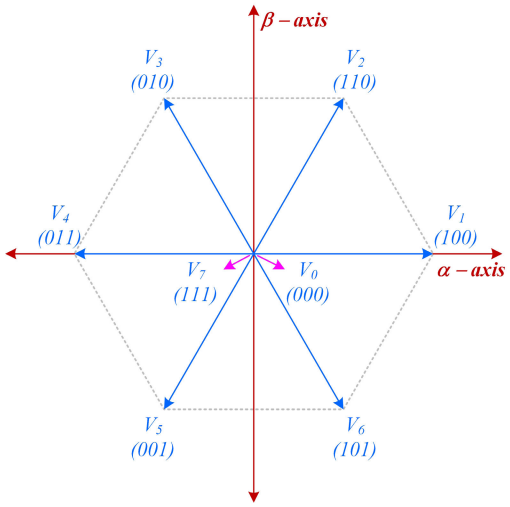

FIGURE 3. Schematic of the 2L-VSI voltage vectors.

possible inverter switching states are displayed in Fig. 3, and the eight possible voltage vectors with their respective voltage states are listed in Table 1.

Out of the eight vectors, six of these (V_1-V_6) are active vectors, and the other two vectors (V_0 and V_7) are null vectors. The voltage and current variables of the three-phase system can be represented by a three-axis coordinate system (abc), as follows:

$$v_{sabc} = \begin{bmatrix} v_{sa} & v_{sb} & v_{sc} \end{bmatrix}^T \tag{4}$$

$$i_{sabc} = \begin{bmatrix} i_{sa} & i_{sb} & i_{sc} \end{bmatrix}^T \tag{5}$$

Furthermore, the relation between the inverter output voltage applied to the IM, with respect to the DC-link voltage, V_{dc}, [45], [46], and the switching functions, S_a, S_b, and S_c, are presented in (6), as follows:

$$v_{sabc} = \begin{bmatrix} S_a & S_b & S_c \end{bmatrix}^T \frac{V_{dc}}{2} \tag{6}$$

Additionally, the stator voltage in two-dimensions in the $\alpha\beta$ stationary reference frame [49], [50] is presented in (7), as follows:

$$v_{\alpha\beta} = \begin{bmatrix} v_{s\alpha} \\ v_{s\beta} \end{bmatrix} = \begin{bmatrix} \frac{3}{2} & -\frac{1}{3} & -\frac{1}{3} \\ 0 & \frac{\sqrt{3}}{3} & \frac{\sqrt{3}}{3} \end{bmatrix} \begin{bmatrix} v_{sa} \\ v_{sb} \\ v_{sc} \end{bmatrix} \tag{7}$$

TABLE 1. Switching states with selected voltages of 2L-VSI.

Voltage Vectors	Voltages in $\alpha\beta$ Frame		Switching States		
	$v_{s\alpha}$	$v_{s\beta}$	S_a	S_b	S_c
V_0	0	0	0	0	0
V_1	$\frac{2}{3}V_{dc}$	0	1	0	0
V_2	$\frac{1}{3}V_{dc}$	$\frac{1}{\sqrt{3}}V_{dc}$	1	1	0
V_3	$-\frac{1}{3}V_{dc}$	$\frac{1}{\sqrt{3}}V_{dc}$	0	1	0
V_4	$-\frac{2}{3}V_{dc}$	0	0	1	1
V_5	$-\frac{1}{3}V_{dc}$	$-\frac{1}{\sqrt{3}}V_{dc}$	0	0	1
V_6	$\frac{1}{3}V_{dc}$	$-\frac{1}{\sqrt{3}}V_{dc}$	1	0	1
V_7	0	0	1	1	1

III. DESIGN OF ISTSMC FOR MODEL PREDICTIVE IM TORQUE CONTROL

A conventional DTC uses a hysteresis control loop. The key difference between the conventional DTC and the MPC-based DTC is that when MPC is used, the switching-table-based hysteresis control is replaced by an algorithm for switching signal calculation. A discrete IM model is used to pre-calculate the behavior of current and flux in next sample interval. The calculated values of current and flux are then fed to an optimizer along with a reference value obtained from the proposed controller in the external loop. The optimizer generates the optimal switching states corresponding to the global minimum cost function in each sampling interval and passes it on to the gate drive of the inverter.

A. MODEL PREDICTIVE TORQUE CONTROL

Standard MPTC schemes linearly combine objective functions to formulate a single cost function that contains flux and torque error, and can be used to select the optimal switching state for the next sampling time. A weighting factor is also incorporated. These factors, which depend on system parameters and operating points, regulate the relative importance of stator flux and torque and, therefore, significantly influence controller performance [28].

The following steps are identified in finite set MPTC design:

- Power inverter modeling to identify all the possible switching states and their relations to output and input currents and voltages
- Defining a cost function to properly represent the desired system behavior
- A discrete-time model formulation that will predict the behavior of control variables, such as torque and flux

To acquire a discrete-time model of the system from the approximation of derivatives, the most common method is the Euler's discretization, which uses:

$$\frac{dx}{dt} = \frac{x(k+1) - x(k)}{T_s} \tag{8}$$

where T_s is the sampling time.

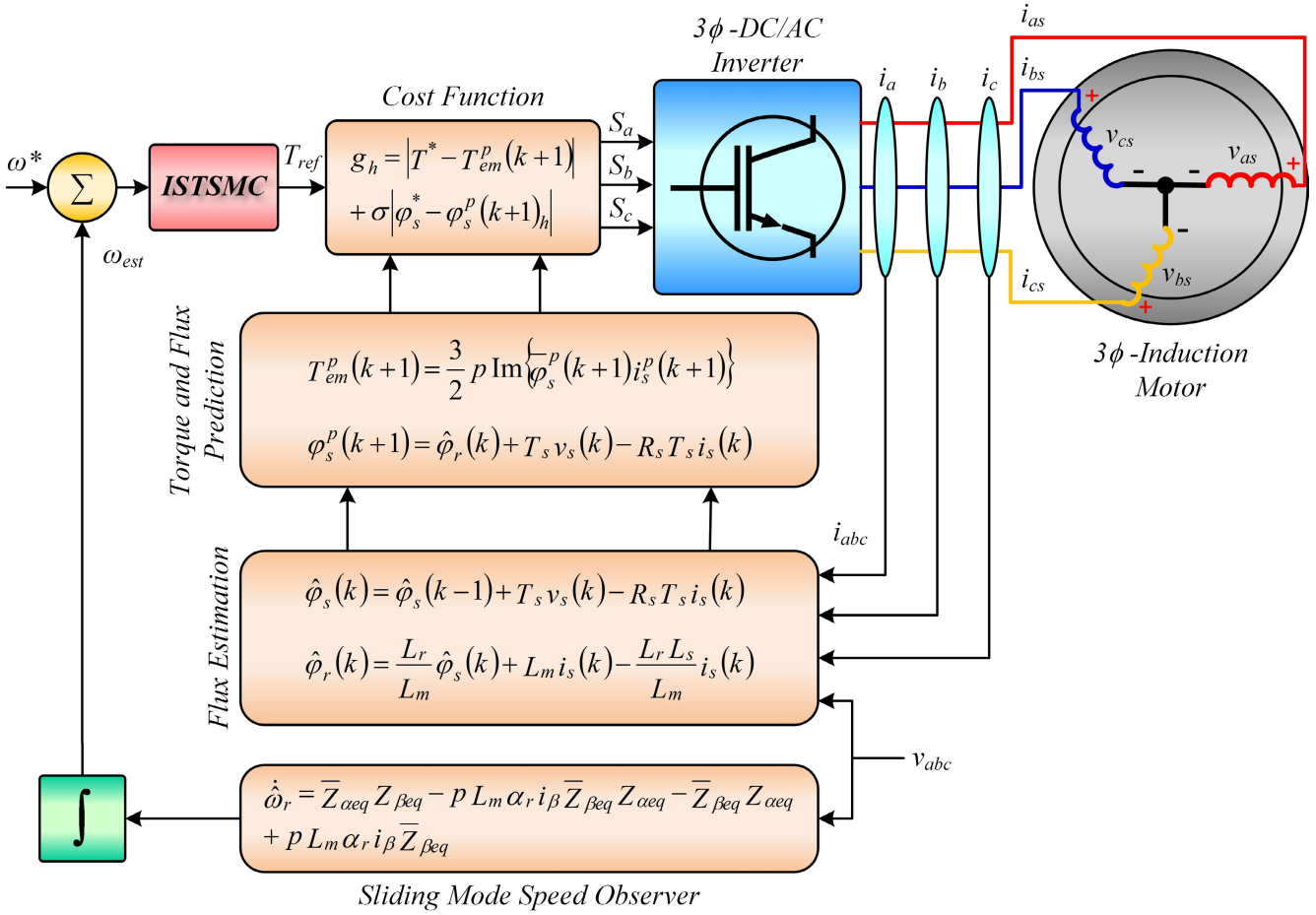

FIGURE 4. Proposed ISTSMC-based sensorless MPTC drive system.

After its initial design, the MPTC scheme must:

- Generate all the possible switching states
- Predict torque and flux behavior for all switching states
- Evaluate the cost function
- Select possible switching states that minimize the cost function
- Select the voltage vector for the corresponding switching states

The complete structure and operation of the proposed ISTSMC-based MPTC scheme is shown in Fig. 4.

1) PREDICTIVE MODEL FOR STATOR CURRENT AND FLUX

The predicted value of stator current in the next time sample is determined using the Euler approximation, which yields (9) when applied to the current, as follows:

$$\left.\begin{aligned} i_\alpha(k+1) &= i_\alpha(k) - \frac{T_s}{\epsilon}\left(\frac{L_m^2\alpha_r + L_r R_s}{L_m}\right) i_\alpha(k) \\ &+ p\omega_r(k)\varphi_\beta + \alpha_r\varphi_\alpha + \frac{L_r}{L_m} v_\alpha(k) \\ i_\beta(k+1) &= i_\beta(k) - \frac{T_s}{\epsilon}\left(\frac{L_m^2\alpha_r + L_r R_s}{L_m}\right) i_\beta(k) \\ &+ p\omega_r(k)\varphi_\alpha + \alpha_r\varphi_\beta + \frac{L_r}{L_m} v_\beta(k) \end{aligned}\right\} \quad (9)$$

where $i_\alpha(k+1)$ and $i_\beta(k+1)$ denote the predicted values of the stator current at $(k+1)th$ time sample.

The stator voltage (v_s) equation is used to estimate the stator flux given as follows:

$$v_s = R_s i_s + \frac{d\varphi_s}{dt} \quad (10)$$

where i_s and φ_s denote the stator current and stator flux, respectively. The Euler's approximation is applied to (10) to estimate the stator flux, as follows:

$$\widehat{\varphi}_s(k) = \widehat{\varphi}_s(k-1) + T_s v_s(k) - R_s T_s i_s(k) \quad (11)$$

where $\widehat{\varphi}_s(k)$ is the estimated stator flux. Additionally, the rotor flux (φ_r) is given by:

$$\varphi_r = L_m i_s + i_r L_r \quad (12)$$

where i_r represents the rotor current. The Euler's approximation is then applied to (12) to estimate the rotor flux, $\widehat{\varphi}_r(k)$, given as:

$$\widehat{\varphi}_r(k) = \frac{L_r}{L_m}\widehat{\varphi}_s(k) + L_m i_s(k) - \frac{L_r L_s}{L_m} i_s(k) \quad (13)$$

The predicted stator flux, ($\varphi_s^p(k+1)$), value is required for the control variables that is calculated using (10) and is represented as:

$$\varphi_s^p(k+1) = \widehat{\varphi}_r(k) + T_s v_s(k) - R_s T_s i_s(k) \quad (14)$$

The stator current, stator flux, and torque are directly interrelated as follows:

$$T_{em} = \frac{3}{2} p \,\mathrm{Im}\left\{\overline{\varphi}_s i_s\right\} \tag{15}$$

Thus, the predicted values of the stator current and stator flux given by (9) and (14), respectively, can be used to predict the torque as follows:

$$T^p_{em}(k+1) = \frac{3}{2} p \,\mathrm{Im}\left\{\overline{\varphi}^p_s(k+1) i^p_s(k+1)\right\} \tag{16}$$

The stator flux and torque values depend on the inverter voltage $V_s(k)$. In a two-level inverter, eight different switching states generate seven voltage levels, and the corresponding flux ($\varphi_s(k+1)_h$) and torque ($T_{em}(k+1)_h$) predictions are acquired using these voltage vectors, where h is between 0 and 6.

Additionally, the cost function has the following structure:

$$g_h = \left|T^* - T^p_{em}(k+1)\right| + \sigma \left|\varphi^*_s - \varphi^p_s(k+1)_h\right| \tag{17}$$

B. FIRST-ORDER SLIDING MODE CONTROL

The IM speed dynamics from (3) is represented as:

$$\dot{\omega}_r = bT_{em} - a\omega_r - f \tag{18}$$

Applying uncertainties Δa, Δb, and Δf in terms a, b, and f, respectively, in (18), we obtain:

$$\dot{\omega}_r = (b+\Delta b)T_{em} - (a+\Delta a)\omega_r - (f+\Delta f) \tag{19}$$

$$\dot{\omega}_r = bT_{em} - a\omega_r - f + d(t) \tag{20}$$

where $d(t) = (\Delta b)T_{em} - (\Delta a)\omega_r - (\Delta f)$ is the system disturbance. The sliding surface, S_1, is selected as the error, $e(t)$, between the reference speed and the actual speed, as follows:

$$S_1(t) = e(t) = \omega_r(t) - \omega_{ref}(t) \tag{21}$$

Using (20), the derivative of the surface is:

$$\dot{S}_1(t) = \dot{e}(t) = bT_{em} - a\omega_r - f + d(t) - \dot{\omega}_{ref}(t) \tag{22}$$

Based on the SM theory, the reference torque can be given as:

$$T_{SMC} = T_{eeq} + T_m \tag{23}$$

The equivalent control part, T_{eeq}, is obtained by taking $\dot{S}_1(t) = 0$, and rearranging for T_{em} as follows:

$$T_{eeq} = \frac{1}{b}\Big[a\omega_r + f + \dot{\omega}_{ref}(t)\Big] - \frac{d(t)}{b} \tag{24}$$

Further, the discontinuous part is defined as:

$$T_m = -\frac{k}{b}\,\mathrm{sgn}\left(S_1(t)\right) \tag{25}$$

Finally, putting the values of T_{eeq} and T_m, from (24) and (25), respectively, into (23) and removing the disturbance term, we obtain:

$$T_{SMC} = \underbrace{\frac{1}{b}\Big[a\omega_r + f + \dot{\omega}_{ref}(t)\Big]}_{T_{eeq}} - \underbrace{\frac{1}{b}\Big[k\,\mathrm{sgn}\left(S_1(t)\right)\Big]}_{T_m} \tag{26}$$

C. INTEGRAL SMC

The sliding phase is responsible for conventional SMC robustness, which is not guaranteed in the reaching phase against load disturbances and parameter variations. To address this, Utkin *et al.* proposed the integral sliding mode control (ISMC) [51]. They eliminated the reaching phase by enforcing the sliding phase in the overall system response, while maintaining the original system order. The main factor responsible for the robustness is the control law, containing both discontinuous and continuous control. Based on the theory of ISMC, a new surface is selected as follows:

$$S_2(t) = e(t) - \int_0^t \gamma e(\tau) d\tau \tag{27}$$

where γ is a positive control gain parameter. The derivative of the proposed surface is:

$$\dot{S}_2(t) = \dot{e}(t) - \gamma e(t) \tag{28}$$

Substituting the values of $\dot{e}(t)$ from (22) in (28), it yields:

$$\dot{S}_2(t) = bT_{em} - a\omega_r - f + d(t) - \dot{\omega}_{ref}(t) - \gamma e(t) \tag{29}$$

Then, the new control input, T_{ISMC}, for ISMC is chosen as:

$$T_{ISMC} = T_{eeq} + T_m \tag{30}$$

Finally, following the steps presented in (23)–(25), the new robust control law is derived as follows:

$$T_{ISMC} = \underbrace{\frac{1}{b}\Big[a\omega_r + f + \dot{\omega}_{ref}(t) + \gamma e(t)\Big]}_{T_{eeq}} \underbrace{-\frac{1}{b}\Big[k\,\mathrm{sgn}\left(e(t) - \int_0^t \gamma e(\tau) d\tau\right)\Big]}_{T_m} \tag{31}$$

1) STABILITY ANALYSIS FOR INTEGRAL SMC

Consider a Lyapunov function, V_{ISMC}, as follows:

$$V_{ISMC} = \frac{1}{2} S_2^2(t) \tag{32}$$

The stability condition for the proposed system is:

$$\dot{V}_{ISMC} = S_2(t)\dot{S}_2(t) \leq 0 \tag{33}$$

A new sliding surface, using the PI combination, is given by:

$$S_2(t) = e(t) - \int_0^t \gamma e(\tau) d\tau \tag{34}$$

While the derivative of the sliding surface is:

$$\dot{S}_2(t) = bT_{em} - a\omega_r - f + d(t) - \dot{\omega}_{ref}(t) - \gamma e(t) \tag{35}$$

Now, substituting the value of $\dot{S}_2(t)$ from (35) in (33) we get:

$$\dot{V}_{ISMC} = S_2(t)\Big[bT_{em} - a\omega_r - f + d(t) - \dot{\omega}_{ref}(t) - \gamma e(t)\Big] \leq 0 \tag{36}$$

For guaranteeing the closed-loop system stability, substituting the value of T_{ISMC} for T_{em}, from (31) in (36), we get:

$$\dot{V}_{ISMC} = S_2(t)\Big[\Big(a\omega_r + f + \dot{\omega}_{ref}(t) + \gamma e(t)\Big) - k\,\mathrm{sgn}\left(e(t) - \int_0^t \gamma e(\tau)d\tau\right) - a\omega_r - f + d(t) - \dot{\omega}_{ref} - \gamma e(t)\Big] \le 0 \quad (37)$$

After simplifications, we get:

$$\dot{V}_{ISMC} = -kS_2(t)\,\mathrm{sgn}\,(S_2(t)) + S_2(t)d(t) \le 0 \quad (38)$$

$$\dot{V}_{ISMC} = -k|S_2(t)| + S_2(t)d(t) \le 0 \quad (39)$$

Hence, for $k \gg \|d(t)\|$ and as time tends to infinity, the proposed system is stable, and the stability condition given in (33) is achieved (i.e. $\dot{V}_{ISMC} \le 0$).

D. INTEGRAL SUPERTWISTING SMC

A new strategy to improve ISMC performance, specifically for rejecting disturbance and minimizing chattering, by combining ISMC and STC, is proposed here. Combining the equivalent control part of ISMC and the discontinuous control part of STC, a new ISTSMC law can be obtained as follows:

$$T_{eRef} = T_{eeq} + U_{ST} \quad (40)$$

where T_{eeq} is defined in (31), and

$$\left.\begin{aligned} U_{ST} &= \frac{1}{b}\left[-\lambda_\omega\sqrt{|S_2(t)|}\,\mathrm{sgn}\,(S_2(t)) + u_1\right] \\ \dot{u}_1 &= -\beta_\omega\,\mathrm{sgn}\,(S_2(t)) \end{aligned}\right\} \quad (41)$$

Hence,

$$U_{ST} = \frac{1}{b}\left[-\lambda_\omega\sqrt{|S_2(t)|}\,\mathrm{sgn}\,(S_2(t)) - \beta_\omega\int_0^t \mathrm{sgn}\,(S_2(\tau)d\tau)\right] \quad (42)$$

Here, the gain β_ω and λ_ω are given as:

$$\left.\begin{aligned} \beta_\omega &> \frac{\emptyset}{\beth_M} \\ \lambda_\omega &\ge \frac{4\emptyset\beth_M\,(\beta_\omega + \emptyset)}{\beth_m^3\,(\beta_\omega - \emptyset)} \end{aligned}\right\} \quad (43)$$

where $\emptyset$ defines the positive bounds of the uncertain function Φ, and $\beth_M$ and $\beth_m$ are the upper and lower positive bounds of the uncertain function μ at the second derivative of the sliding manifold, respectively, which is ω_r in this case. Furthermore:

$$\emptyset \ge \Phi \quad \text{and} \quad \beth_M \ge \mu \ge \beth_m \quad (44)$$

$$\ddot{\omega}_r = \Phi(x,t) + \mu(x,t)\dot{u} \quad (45)$$

where $\emptyset$, $\beth_M$ and $\beth_m$ are considered as positives constants. Thus, the proposed control law using the sliding surface given in (27), will have the following structure:

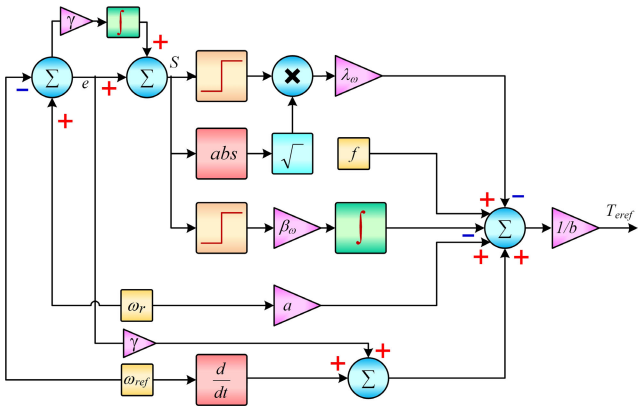

FIGURE 5. Operational diagram of the proposed ISTSMC.

$$T_{eRef} = \underbrace{\frac{1}{b}\Big[a\omega_r + f + \dot{\omega}_{ref}(t) + \gamma e(t)\Big]}_{T_{eeq}} + \underbrace{\frac{1}{b}\left[-\lambda_\omega\sqrt{|S_2(t)|}\,\mathrm{sgn}\,(S_2(t)) - \int_0^t \beta_\omega\,\mathrm{sgn}\,(S_2(t))\right]}_{U_{ST}} \quad (46)$$

The ISTSMC-based law must fulfill the Lyapunov stability theory, and the Lyapunov-based stability of the proposed control law is, therefore, discussed in the next section. The implementation strategy of the proposed ISTSMC controller is illustrated in Fig. 5. Herein, a standard STC algorithm presented in [52], [53] is considered to prove the stability of the closed-loop system. Additionally, a new space vector is introduced as:

$$\left.\begin{aligned} z_{ST} &= (z_1, z_2)^T = \left(\lambda_\omega\sqrt{|S_2(t)|}\,\mathrm{sgn}\,(S_2(t)), u_1\right) \\ \dot{u}_1 &= -\beta_\omega\,\mathrm{sgn}\,(S_2(t)) \end{aligned}\right\} \quad (47)$$

A Lyapunov stability function V_{ISTC} is selected to prove the stability of the proposed controller:

$$V_{ISTC} = \frac{1}{2}z_{ST}^T Q z_{ST} \quad (48)$$

where Q is a positive matrix defined as:

$$Q = \begin{bmatrix} q_{11} & q_{12} \\ q_{21} & q_{22} \end{bmatrix} \quad (49)$$

The derivative of (48) and the stability condition can be presented together as:

$$\dot{V}_{ISTC} = z_{ST}^T Q \dot{z}_{ST}^T \le 0 \quad (50)$$

The solution of a quadratic algebraic Lyapunov equation (ALE) [54] is given as:

$$A^T Q + QA = -P \quad (51)$$

where $P = P^T > 0$ and A is Hurwitz, defined as:

$$A = \begin{bmatrix} -\frac{1}{2}\lambda_\omega & \frac{1}{2} \\ -\beta_\omega & 0 \end{bmatrix} \quad (52)$$

Hence, using the solution given in (51) and substituting the value of z_{ST} into (49), $\dot{V}_{ISTC}$ in (50) can be written as:

$$\left.\begin{aligned}\dot{V}_{ISTC} &= \frac{-1}{\sqrt{|S(t)|}} z_{ST}^T \left[-A^T Q - QA\right] \dot{z}_{ST} \\ \dot{V}_{ISTC} &= \zeta_{min} \left[-A^T Q - QA\right] \frac{1}{\sqrt{\zeta_{min}}} Q \| z_{ST}^T \| \leq 0\end{aligned}\right\} \tag{53}$$

where $\frac{1}{\sqrt{|S(t)||}} \neq 0$ and the matrix $A^T Q + QA$ can be forced to be negative by solving the linear matrix inequality (LMI) as follows:

$$A^T Q + QA < 0 \tag{54}$$

Hence, a stable condition for the proposed control paradigm has been established.

IV. DESIGN OF SLIDING MODE SPEED OBSERVER

Conventional SM strategies have a key discontinuous feature, with external disturbance control and inaccuracy management build into the model, making the control systems more effective and robust. Thus, an SM system can be designed by considering a single-input and single-output system, $\dot{S} = u$, where u can be selected such that the sliding surface tends to zero ($S \to 0$). The generic form of such an SM is constructed as follows:

$$u = -K \text{ sign } (S) \quad K > 0$$

where K is the gain.

On the basis of the variable structure of the SM theory, the sliding surface is selected as:

$$S_i(t) = \widehat{I}_s - I_s \tag{55}$$

where $\widehat{I}_s = \widehat{i}_\alpha, \widehat{i}_\beta$ are the estimated stator current values and $I_s = i_\alpha, i_\beta$ are the actual stator current values. Based on the IM stator current determined in (1), the SMO is presented as:

$$\left.\begin{aligned}\dot{\widehat{i}}_\alpha &= -\left(\frac{L_m^2 \alpha_r + L_r R_s}{\varepsilon L_m}\right)\widehat{i}_\alpha + \frac{L_r}{L_m} v_{s\alpha} + \alpha_r \varphi_\alpha + Z_\alpha \\ \dot{\widehat{i}}_\beta &= -\left(\frac{L_m^2 \alpha_r + L_r R_s}{\varepsilon L_m}\right)\widehat{i}_\beta + \frac{L_r}{L_m} v_{s\beta} + \alpha_r \varphi_\beta + Z_\beta\end{aligned}\right\} \tag{56}$$

where $Z_\alpha = -K \text{ sgn } \left(\widehat{i}_\alpha - i_\alpha\right)$ and $Z_\beta = -K \text{ sgn } \left(\widehat{i}_\beta - i_\beta\right)$.

A. STABILITY ANALYSIS I

A Lyapunov stability function, V_i, was selected and used to verify the stability of the proposed SMO:

$$V_i = \frac{1}{2} S_i^2(t) \tag{57}$$

The stability of SMO is verified by the Lyapunov stability condition given as:

$$\dot{V}_i = S_i(t) \dot{S}_i(t) \leq 0 \tag{58}$$

The error equations for the estimated currents are obtained by subtracting (1) from (56).

The surface derivative is given as:

$$\left.\begin{aligned}\dot{S}_{i1}(t) &= -\alpha_r S_{i1}(t) + p\omega_r \varphi_\beta + Z_\alpha \\ \dot{S}_{i2}(t) &= -\alpha_r S_{i2}(t) - p\omega_r \varphi_\alpha + Z_\beta\end{aligned}\right\} \tag{59}$$

where

$$S_i(t) = \begin{bmatrix} S_{i1}(t) \\ S_{i2}(t) \end{bmatrix} = \begin{bmatrix} \widehat{i}_\alpha - i_\alpha \\ \widehat{i}_\beta - i_\beta \end{bmatrix} \tag{60}$$

The stability condition given by (58) can be written as:

$$\dot{V}_i = S_i(t) \dot{S}_i(t) = S_{i1}(t) \dot{S}_{i1}(t) + S_{i2}(t) \dot{S}_{i2}(t) \tag{61}$$

and substituting the values of $S_{i1}(t)$, $\dot{S}_{i1}(t)$, $S_{i2}(t)$, and $\dot{S}_{i2}(t)$ in (61), it yields:

$$\begin{aligned}\dot{V}_i = -K\Big[&\left(\widehat{i}_\alpha - i_\alpha\right) \text{sign}\left(\widehat{i}_\alpha - i_\alpha\right) + \left(\widehat{i}_\beta - i_\beta\right) \text{sign}\left(\widehat{i}_\beta \right. \\ &\left. - i_\beta\right)\Big] - \alpha_r\Big[\left(\widehat{i}_\alpha - i_\alpha\right)^2 + \left(\widehat{i}_\beta - i_\beta\right)^2\Big] \\ &+ p\omega_r\Big[\widehat{i}_\alpha i_\beta - \widehat{i}_\beta i_\alpha\Big]\end{aligned} \tag{62}$$

This shows that a large enough value of K ensures the existence and stability, given in (58), of the SMO. Once the sliding surface is reached, then:

$$S_i(t) = \dot{S}_i(t) = 0 \tag{63}$$

The desired SM dynamics can be achieved by putting $\dot{S}_i(t) = S_i(t) = 0$ into (56) and replacing the discontinuous functions Z_α and Z_β with their equivalent control components $Z_{\alpha eq}$ and $Z_{\beta eq}$. Thus,

$$\left.\begin{aligned}Z_{\alpha eq} &= p\omega_r \varphi_\beta \\ Z_{\beta eq} &= -p\omega_r \varphi_\alpha\end{aligned}\right\} \tag{64}$$

In this case, $Z_{\alpha eq}$ and $Z_{\beta eq}$ can be obtained from the discontinuous terms Z_α and Z_β by using a low pass filter (LPF), as presented in detail in [55].

Taking derivatives of (64), we have

$$\left.\begin{aligned}\dot{Z}_{\alpha eq} &= p\omega_r \dot{\varphi}_\beta + p\dot{\omega}_r \varphi_\beta \\ \dot{Z}_{\beta eq} &= p\omega_r \dot{\varphi}_\alpha + p\dot{\omega}_r \varphi_\alpha\end{aligned}\right\} \tag{65}$$

Assumption A1: The IM rotor speed dynamics vary too slowly to impact the stator current and rotor flux dynamics, therefore, it can be assumed that $\dot{\omega}_r = 0$.

The IM electric variables are represented in (1) and (2), while (3) demonstrates the relationship between speed and torque. The rotor speed depends on the electric torque, f, the load torque and J. The dynamics of f and J are much slower than the other electrical dynamics, therefore, the rotor speed dynamic behavior is similar to that of the LPF. Additionally, the rotor speed can be assumed to be constant compared to the electrical variable dynamics [24]. Hence, based on *Assumption A1*, (65) can be written as:

$$\left.\begin{aligned}\dot{Z}_{\alpha eq} &= p\omega_r \dot{\varphi}_\beta \\ \dot{Z}_{\beta eq} &= -p\omega_r \dot{\varphi}_\alpha\end{aligned}\right\} \tag{66}$$

Putting the values of $\dot{\varphi}_\beta$ and $\dot{\varphi}_\alpha$, from (2), into (66) we get:

$$\left.\begin{aligned}\dot{Z}_{\alpha eq} &= p\omega_r \left(L_m \alpha_r i_\beta + p\omega_r \varphi_\alpha - \alpha_r \varphi_\beta\right) \\ \dot{Z}_{\alpha eq} &= -\alpha_r Z_{\alpha eq} - p\omega_r Z_{\beta eq} + pL_m \omega_r \alpha_r i_\beta\end{aligned}\right\} \tag{67}$$

Similarly, we have

$$\left.\begin{aligned}\dot{Z}_{\beta eq} &= -p\omega_r\left(L_m\alpha_r i_\alpha - p\omega_r\varphi_\beta - \alpha_r\varphi_\alpha\right)\\ \dot{Z}_{\beta eq} &= -\alpha_r Z_{\beta eq} + p\omega_r Z_{\alpha eq} - pL_m\omega_r\alpha_r i_\alpha\end{aligned}\right\} \quad (68)$$

Based on the Leuenberger observer theory, an observer designed for the variables in (67) and (68), is represented as:

$$\left.\begin{aligned}\hat{\dot{Z}}_{\alpha eq} &= -\alpha_r Z_{\alpha eq} - p\widehat{\omega}_r Z_{\beta eq} + pL_m\widehat{\omega}_r\alpha_r i_\beta - L\overline{Z}_{\alpha eq}\\ \hat{\dot{Z}}_{\beta eq} &= -\alpha_r Z_{\beta eq} + p\widehat{\omega}_r Z_{\alpha eq} - pL_m\widehat{\omega}_r\alpha_r i_\alpha - L\overline{Z}_{\beta eq}\end{aligned}\right\} \quad (69)$$

where

$$\left.\begin{aligned}\overline{Z}_{\alpha eq} &= \widehat{Z}_{\alpha eq} - Z_{\alpha eq}\\ \overline{Z}_{\beta eq} &= \widehat{Z}_{\beta eq} - Z_{\beta eq}\\ \overline{\omega}_r &= \widehat{\omega}_r - \dot{\omega}_r\end{aligned}\right\}$$

B. STABILITY ANALYSIS II

Importantly, the Lyapunov stability must be evaluated here as well. The Lyapunov function is depicted as follows:

$$V_\omega = \frac{1}{2}\left(\overline{Z}^2_{\alpha eq} + \overline{Z}^2_{\beta eq} + \overline{\omega}^2_r\right) \quad (70)$$

Taking the derivative of (70), we get:

$$\dot{V}_\omega = \overline{Z}_\alpha\dot{\overline{Z}}_{\alpha eq} + \overline{Z}_\beta\dot{\overline{Z}}_{\beta eq} + \overline{\omega}_r\dot{\overline{\omega}}_r \quad (71)$$

where

$$\left.\begin{aligned}\dot{\overline{Z}}_{\alpha eq} &= -pZ_{\beta eq}\overline{\omega}_r + pL_m\alpha_r i_\beta\overline{\omega}r - \overline{L}Z_{\alpha eq}\\ \dot{\overline{Z}}_{\beta eq} &= -pZ_{\alpha eq}\overline{\omega}_r + pL_m\alpha_r i_\beta\overline{\omega}_r - L\overline{Z}_{\beta eq}\end{aligned}\right\} \quad (72)$$

Substituting (72) into (71) and applying the stability condition $\dot{V}_\omega \le 0$, we have:

$$-L\left(\overline{Z}^2_{\alpha eq} - \overline{Z}^2_{\beta eq}\right) < 0 \quad (73)$$

$$-\overline{Z}_{\alpha eq}Z_{\beta eq}\overline{\omega}_r + pL_m\alpha_r i_\beta\overline{\omega}_r\overline{Z}_{\alpha eq} + \overline{Z}_{\beta eq}Z_{\alpha eq}\overline{\omega}_r - pL_m\alpha_r i_\beta\overline{\omega}_r\overline{Z}_{\beta eq} + \overline{\omega}\,\dot{\overline{\omega}} = 0 \quad (74)$$

Using (74), and solving for estimated speed, we determine the required speed, which is given by:

$$\left.\begin{aligned}\widehat{\omega}_r &= \overline{Z}_{\alpha eq}Z_{\beta eq} - pL_m\alpha_r i_\beta\overline{Z}_{\alpha eq} - \overline{Z}_{\beta eq}Z_{\alpha eq} + pL_m\alpha_r i_\beta\overline{Z}_{\beta eq}\\ \widehat{\omega}_r &= \int\left(\overline{Z}_{\alpha eq}Z_{\beta eq} - pL_m\alpha_r i_\beta\overline{Z}_{\alpha eq} - \overline{Z}_{\beta eq}Z_{\alpha eq} + pL_m\alpha_r i_\beta\overline{Z}_{\beta eq}\right)dt\end{aligned}\right\} \quad (75)$$

Thus, the rotor speed is estimated using (75). It is clear from (73) that, for large values of L, the observer in (75) is stable and the variables $Z_{\alpha eq}$ and $Z_{\beta eq}$ are close to zero as time approaches infinity. The implementation strategy of the proposed SMO is illustrated in Fig. 6.

V. PERFORMANCE EVALUATION

A. SIMULATION SETUP

The IM control system simulations were performed in MATLAB/Simulink. The load torque variation, single phase fault, and sinusoidal fault perturbations are considered as a disturbance for the IM drive. The algorithm sampling time was a fixed 50 μs time step, implemented with an ode 5 (Dormand-Prince) solver. The comparison of various control techniques depends on the variation of the input reference signal. First, the speed convergnece and robustness of the proposed SMO was investigated. Then the performance of the proposed controller was evaluated using various stability, robustness, and convergence tests and compared with the conventional PI and SMC controllers. The IM and the controller tuning parameters used in simulating PI, SMC, and ISTSMC systems are listed in Table 2.

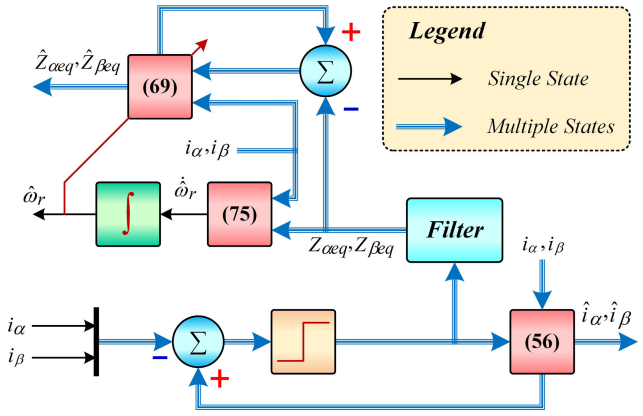

FIGURE 6. Operational diagram of the proposed SMO.

TABLE 2. Induction motor tuning parameters.

IM Parameters	Values	Control Parameters	Values
V_{dc}	520	k	$0.5-5$
p	2	λ_ω	100
R_s	1.40 Ω	β_ω	7
R_r	1.20 Ω	γ	$0.4-4$
L_m	0.20 H	K_p	3.01
L_r	0.175 H	K_i	4.15
L_s	0.18 H	L	300
J	0.07 $kg.m^2$	K	800
...	...	σ	28

B. SLIDING MODE OBSERVER PERFORMANCE

The SMO can be globally stable with sufficiently large gains, such that it can minimize parametric errors, sensor measurements, and other modeled uncertainties. Very large gains make the observer robust against changes in the IM parameters, but they ultimately increase the chattering effects as well. Thus, the value of K and L selected here are 800 and 300, respectively.

In the first test, the rotor reference speed (ω_{ref}) was varied from 0 to 150 rad/s. The resulting response of the proposed observer is depicted in Fig. 7, which verifies that the estimated rotor speed converges to the actual rotor speed and tracks the reference rotor speed with a negligible error. The selected values of K and L, as well as the bandwidth of the chosen LPF, determine the oscillations of the estimated speed. The K gain regulates the convergence of the estimated rotor speed to the actual speed, while the high L gain guarantees fast convergence of estimated current to actual values. The filtered and observed $Z_{\alpha eq}$ values are shown in Fig. 8.

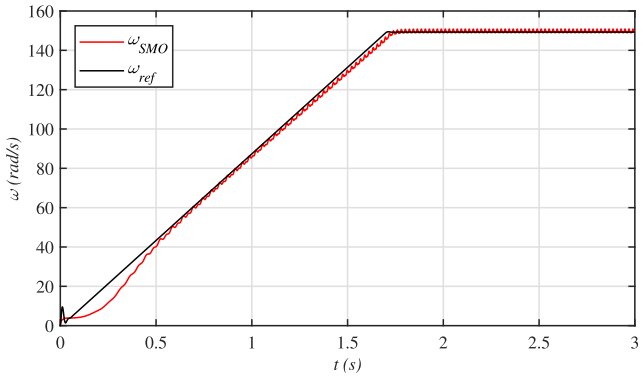

FIGURE 7. Speed observed by the proposed SMO.

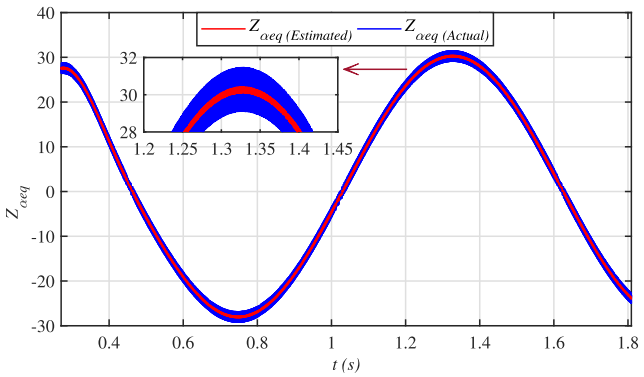

FIGURE 8. Observed and calculated $Z_{\alpha eq}$ values.

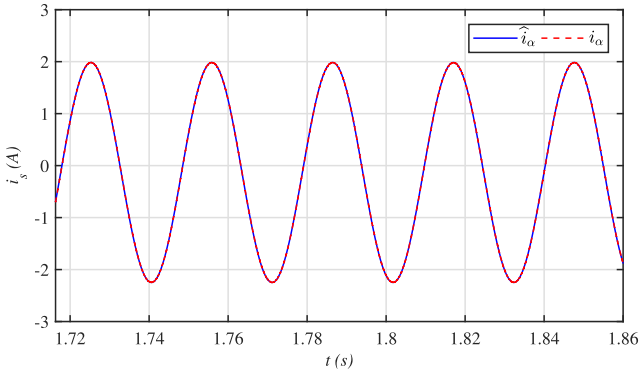

FIGURE 9. Calculated and estimated stator current.

The high-frequency component in $Z_{\alpha eq}$ can be decreased by selecting the appropriate LPF bandwidth. The estimated and actual stator currents, for the $\alpha - axis$, are shown in Fig. 9, where the two coincide with one another.

Next, a variable reference speed that gradually increased from 0 to 100 rad/s was applied to the observer, and Fig. 10 shows the resulting performance of the proposed SMO with reasonable estimation.

C. SPEED RESPONSE UNDER EXTERNAL DISTURBANCES

External disturbances were applied to validate the robustness of both the SMO and the proposed controller. The behavior of the external disturbance, $d(t)$, was assumed to be a sinusoidal wave, and was applied for 20 ms. This sinusoidal disturbance simulated the effects of slow frequencies in the drive

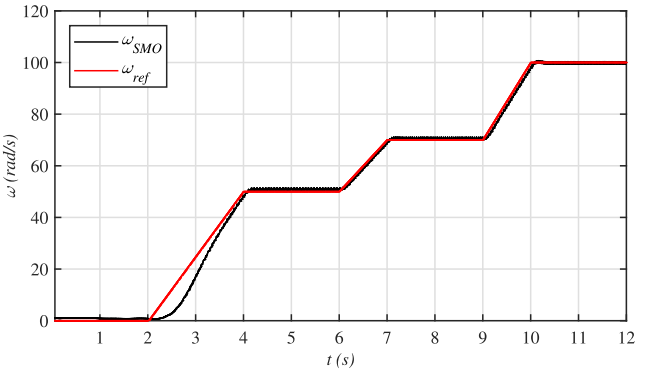

FIGURE 10. Estimated variable speed by the proposed SMO.

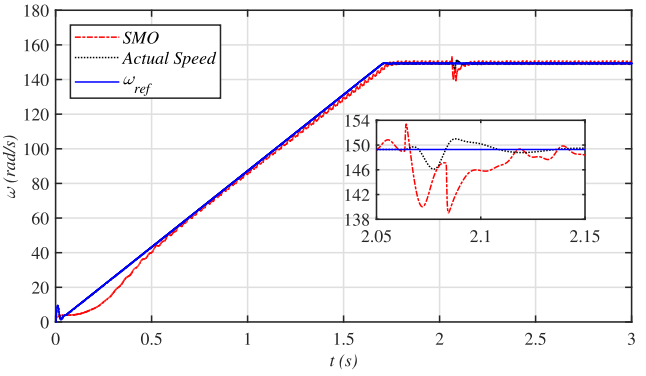

FIGURE 11. Estimated and actual rotor speed response under sinusoidal fault.

system electrical variables. Mathematically, this sinusoidal disturbance is represented as:

$$\left.\begin{aligned}\dot{\omega}_r &= bT_{em} - a\omega_r - f + d(t)\\ d(t) &= 20sin(\omega t) + 10\end{aligned}\right\}$$

The response of the proposed sensorless system under the sinusoidal disturbance is shown in Fig. 11. The rotor speed converges to the reference speed in 30 ms, while the observer convergence time is 40 ms after the disturbance, $d(t)$, is applied. Clearly, the proposed control system and observation topology are quite fast, in addition to being robust to the external disturbances.

D. PERFORMANCE ANALYSIS OF PROPOSED CONTROLLER IN CONSTANT SPEED OPERATION

In this case, a constant speed reference of 150 rad/s was used to validate the speed tracking of the PI, SMC, and proposed controller, with the resulting waveforms shown in Fig. 12. The PI controller completely converges at 0.7 s, and its speed waveform has an overshoot and undershoot of 42.7 and 6 rad/s, respectively. The SMC controller converges at 0.25 s, and provides an overshoot and undershoot of 0.5 and 0.266 rad/s, respectively. Our proposed controller confirms its fast convergence at 0.087 s and has an overshoot of 0.002 rad/s. An increase in the oscillation speed, between 150.05 and 149.9 rad/s, is also observed in Fig. 12 for the SMC controller due to chattering problems. The proposed controller completely eliminates the IM speed oscillations,

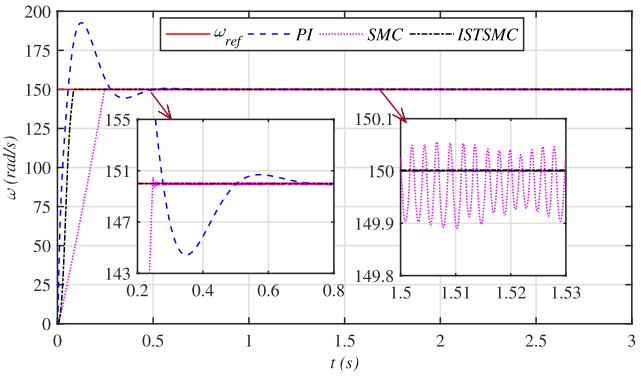

FIGURE 12. Speed response of PI, SMC, and the proposed ISTSMC.

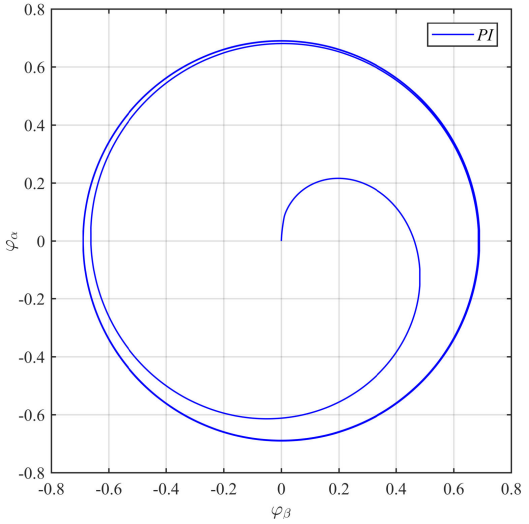

FIGURE 13. Stator flux trajectory for PI based MPTC.

thus validating the enhancement achieved in the SMC using a super twisting algorithm.

The stator flux trajectories for the PI, SMC and proposed ISTSMC based MPTC approaches are illustrated in Figs. 13, 14 and 15, respectively, where the SMC based approach exhibits high ripples due to chattering phenomenon. It can clearly be seen that the ISTSMC based approach has much improved flux trajectory when compared with both the PI and SMC based approaches.

The current waveforms for the PI, SMC, and proposed ISTSMC systems are shown in Fig. 16, which demonstrates that the proposed controller also minimizes the current, resulting in fewer copper losses compared to the PI and SMC systems. The SMC has large current waveforms and oscillations, due to the chattering problem, which produce high copper losses. The PI controller has a smoother waveform than the the SMC, but it has a larger starting current than the ISTSMC controller. The control efforts for a constant speed of 150 rad/s are shown in Fig. 17.

The ISTSMC convergence was further validated by applying a series of gradually decreasing constant reference inputs, ranging from 150 to 30 rad/s, shown in Fig. 18. Notably, this system offers superior convergence speeds for both high and low reference speeds.

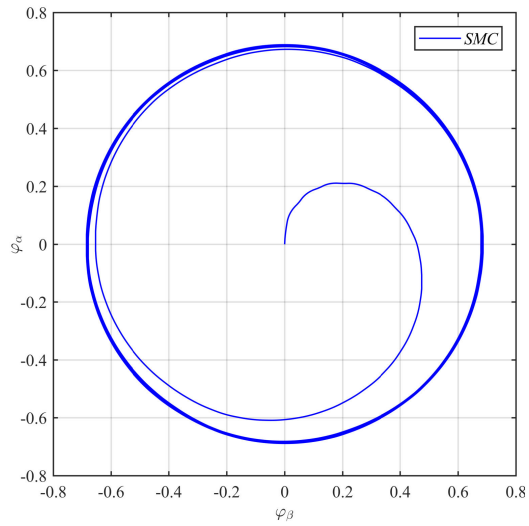

FIGURE 14. Stator flux trajectory for SMC based MPTC.

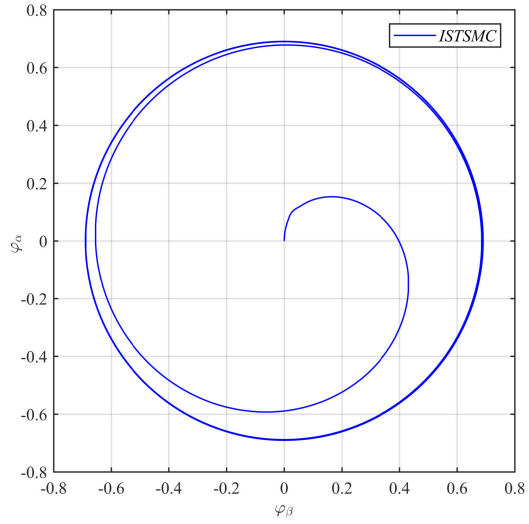

FIGURE 15. Stator flux trajectory for the proposed ISTSMC.

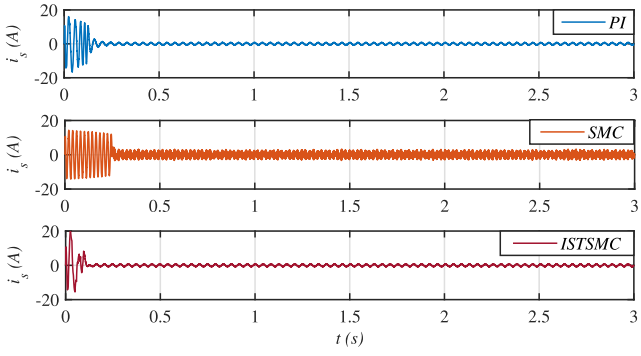

FIGURE 16. Stator phase currents comparison of PI, SMC, and ISTSMC based MPTC.

E. PERFORMANCE ANALYSIS UNDER TORQUE DISTURBANCES

A load of 25 $N.m$ is applied at 1.5 s to create a reference step signal speed that ranges from 150 to -150 rad/s, and the resulting waveform is shown in Fig. 19. The PI, SMC,

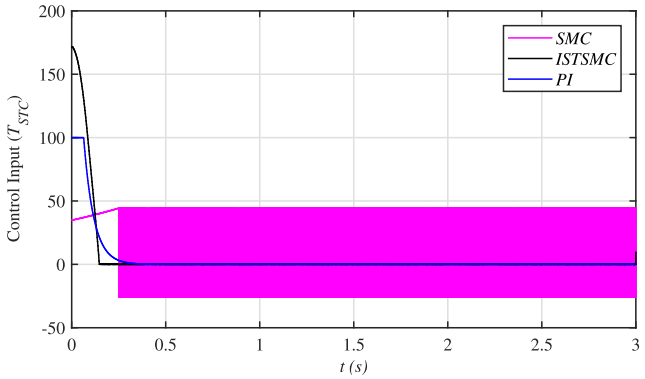

FIGURE 17. Control efforts comparison for constant speed operation.

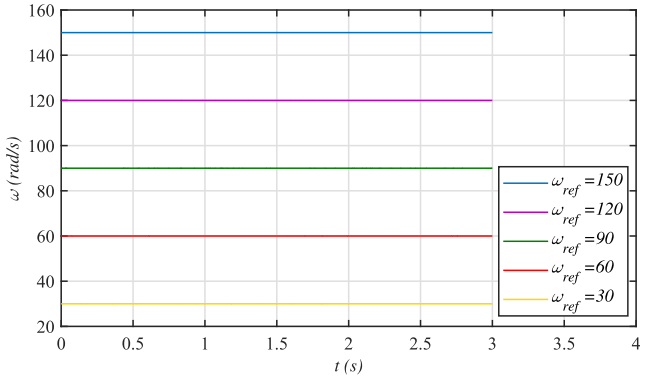

FIGURE 18. Speed convergence plot for the proposed ISTSMC speed controller under various reference speeds.

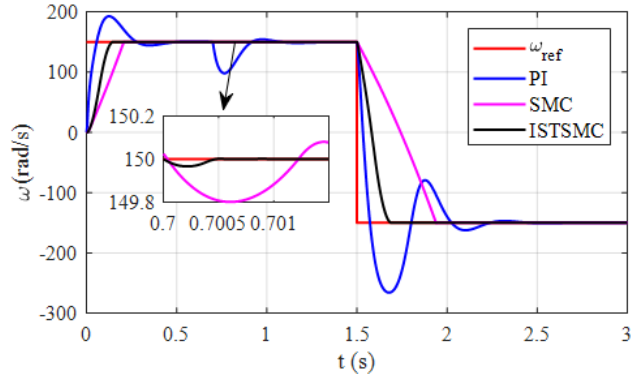

FIGURE 19. Rotor speed response under load disturbances and in reverse operation.

and ISTSMC systems exhibit speed drops of 52, 0.2, and 0.034 rad/s, respectively, when the load is applied. The PI and SMC systems converge completely in 0.7 s and 2.5 ms, respectively. The proposed ISTSMC convergence time of 1 ms is very small compared to the PI and SMC systems. Furthermore, the proposed controller also shows improved performance over the PI and SMC systems in the reverse speed operation region by exhibiting a negligible overshoot and faster convergence.

Variable load torques, that gradually decreased from 10 to -10 $N.m$, and then increased again to 10 $N.m$, were applied to evaluate the IM drive stability and performance

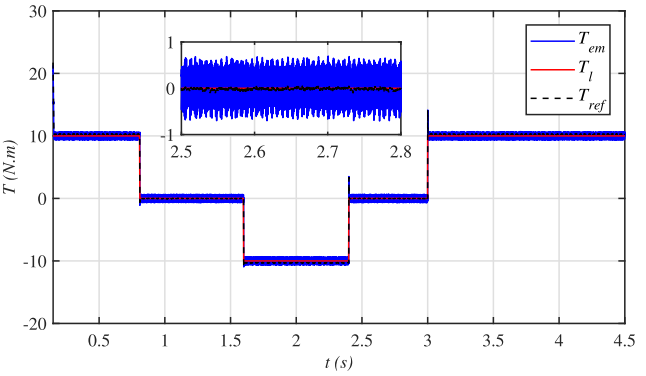

FIGURE 20. Reference torque and actual motor torque under variable load application.

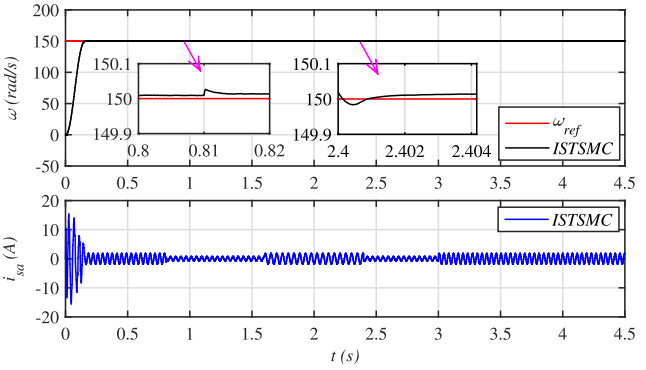

FIGURE 21. Speed and current response of the proposed ISTSMC system under variable torque application.

under various designed control strategies. The applied load torque, T_l, electromagnetic torque, T_{em}, and the reference torque, T_{ref}, are shown in Fig. 20, which verifies that the reference torque generated by the ISTSMC, according to the applied load torque, T_l, is thoroughly followed by the IM drive. Figure 21 shows the response of the ISTSMC controller in terms of speed convergence and current for variable applied torque.

F. TEST FOR ROBUSTNESS AGAINST ELECTRICAL FAULTS

Next, the MPTC-based IM drive was subjected to an open phase fault. In this stage, phase a of the IM is opened at 1.5 s. Figure 22 shows the corresponding speed for all the evaluated controllers. The PI controller loses convergence and stability when subjected to open phase fault, resulting in a highly variable speed, while the SMC system is less severely affected. The proposed ISTSMC exhibits superior stability and high-speed convergence as compared to PI and SMC systems, because it utilizes enhancements made to the generic SMC.

Under these operating conditions, extra current is drawn by phase b and phase c, producing excessive heat in the stator winding. The current behavior in phase b during open phase fault testing is shown in Fig. 23. Clearly, the proposed ISTSMC system surpasses the PI and SMC controllers, as it draws significantly lower currents, subsequently producing less heat at stator winding. The corresponding control efforts

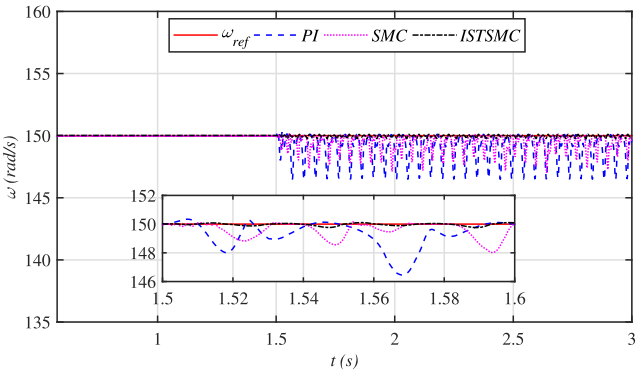

FIGURE 22. Speed response under open phase fault (phase *a* opened).

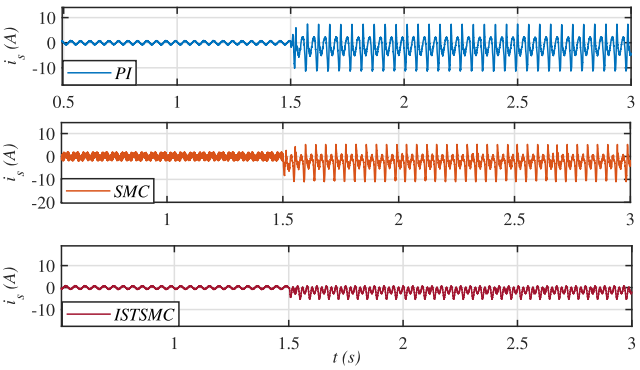

FIGURE 23. Stator phase *b* current comparison under faulty operation.

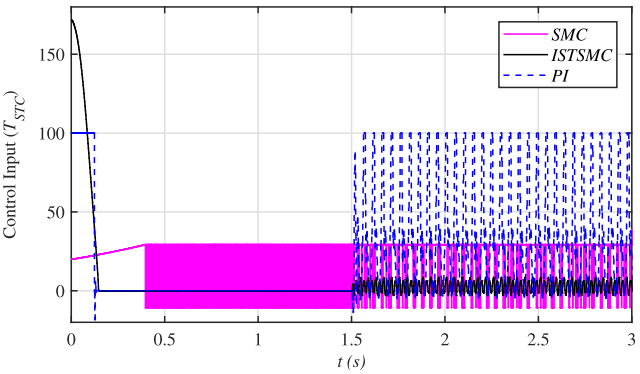

FIGURE 24. control efforts under faulty operation.

for the faulty IM drive are shown in Fig. 24, where it can be seen that the the proposed ISTSMC scheme exerts the lowest control effort during faulty operation.

G. TEST FOR ROBUSTNESS AGAINST PLANT PARAMETRIC UNCERTAINTIES

The robustness of the proposed technique to parametric uncertainties was evaluated by increasing the stator resistance (R_s) to 1.5 and 2 times the base stator resistance, and the resulting speed response is shown in Fig. 25. With respect to the actual rotor speed, the speed variation was 0.008 and 0.012 rad/s for a stator resistance of $1.5 \times R_s$ and $2 \times R_s$, respectively, which is negligibly small. It means that the proposed ISTSMC strategy has significant robustness against stator resistance variation.

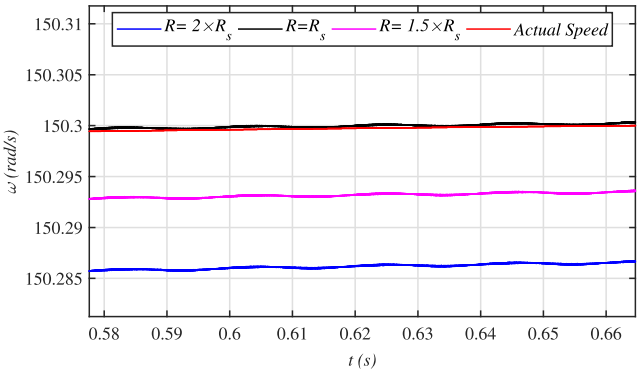

FIGURE 25. Simulated rotor speed response under stator resistance variation.

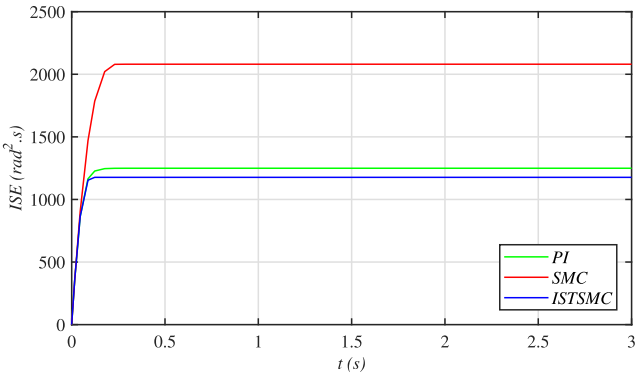

FIGURE 26. Integral of squared error.

H. PERFORMANCE EVALUATION THROUGH VARIOUS INDICES

The proposed controller performance was also evaluated through various performance indices using: (1) integral of square error (*ISE*), (2) integral of time multiplied by squared error (*ITSE*), (3) integral of absolute error (*IAE*), and (4) integral of time multiplied by absolute error (*ITAE*).

The speed error is defined as:

$$e = \left(\omega_{ref} - \omega_{actual}\right) \tag{76}$$

where ω_{ref} is the reference speed and ω_{actual} is the actual speed of the IM. The *ISE*, *ITSE*, *IAE*, and *ITAE* are defined as follows [56]:

$$\left.\begin{aligned} ISE &= \int_0^t e^2(t)dt \\ ITSE &= \int_0^t te^2(t)dt \\ IAE &= \int_0^t |e(t)|dt \\ ITAE &= \int_0^t t|e(t)|dt \end{aligned}\right\} \tag{77}$$

where t denotes the total simulation time.

The *ISE*, *ITSE*, *IAE*, and *ITAE* for a constant input speed of 150 rad/s are shown in Figs. 26-29 respectively. In each case, as the time increases, the accumulative error of each candidate control strategy also increases. However, the proposed ISTSMC strategy renders the flattest error profile and,

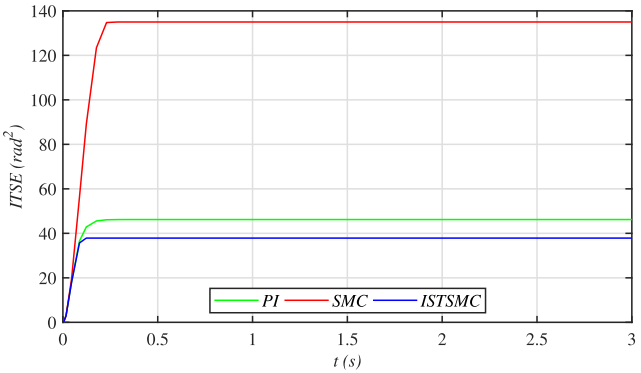

FIGURE 27. Integral of time multiplied by squared error.

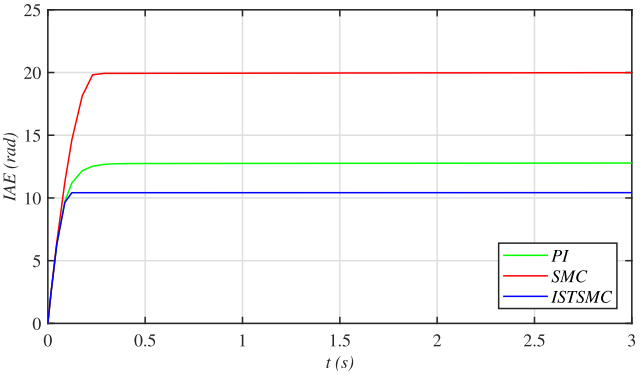

FIGURE 28. Integral absolute error.

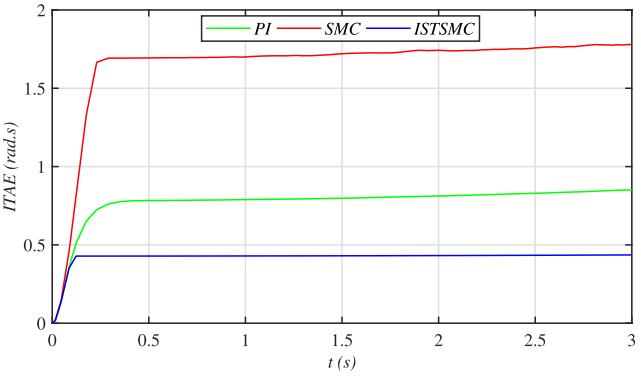

FIGURE 29. Integral of time multiplied by absolute error.

hence, the lowest error, thus, exhibiting the superior performance to its competitors. The PI scheme is the second best candidate, because the PI system is not subjected to inherent chattering. Thus, it exhibits less severe oscillations in the speed waveform and subsequently has lower error as compared to the SMC. On the other hand, the first-order SMC renders the greatest error due to inherent chattering phenomenon.

The overall performance of the three candidate control techniques, evaluated based on the speed convergence time, maximum speed drop when a load is applied, convergence time after load application, and overshoot, is summarized in Table 3. This performance comparison shows the superiority of the proposed ISTSMC for sensorless MPTC over the PI and SMC based MPTC schemes.

TABLE 3. Performance analysis in terms of various dynamics.

Dynamics	PI-MPTC	SMC-MPTC	ISTSMC-MPTC
Speed Convergence Time (s)	0.70	0.266	0.087
Drop in speed when load is applied (rad/s)	52	0.2	0.034
Speed Response Time after applying load (ms)	700	2.50	1
Overshoot (rad/s)	42.70	0.50	0.002

VI. CONCLUSION

This study proposed an MPC based on ISTSMC for high-performance IM control. The method is built on fundamental IM and 2L-VSI equations, and utilizes MPC approaches. The proposed control paradigm is designed by combining the Integral SMC and supertwisting algorithm, which not only solved the problem of chattering but also improved the robustness and stability of the system. The system stability has been mathematically analyzed and proven using the Lyapunov stability theorem, and the ISTSMC-MPTC strategy has been compared with PI-MPTC and SMC-MPTC strategies using various load and faults tests. The simulation results demonstrate the superiority of the proposed method for disturbance rejection, overshoot, load variations, negative speed operation, and fault perturbation. In addition, the proposed SMO provided superior results in closed-loop operation with the ISTSMC controller. Based on the simulation results in this paper, it is clear that the main improvements are:

- Elimination of inherent chattering in conventional SMC
- Fast response of the rotor speed in transient state
- MPTC based on ISTSMC with SMO enables the system to be of very high accuracy, good fastness, and no-overshoot

Overall, the results confirm that the strategy developed in this study provides a very attractive and promising alternative for high-performance AC drives. In the near future, the proposed methodology will be validated using experimental workbench. Furthermore, the robust control paradigms can be further improved by other variants such as fractional order STSMC, fuzzy double hidden layer recurrent neural terminal SMC, adaptive H-infinity control and recurrent neural network fractional order SMC.

REFERENCES

[1] S. Khan, S. S. H. Bukhari, and J.-S. Ro, "Design and analysis of a 4-kW two-stack coreless axial flux permanent magnet synchronous machine for low-speed applications," *IEEE Access*, vol. 7, pp. 173848–173854, 2019.

[2] H.-K. Yeo and J.-S. Ro, "Novel analytical method for overhang effects in surface-mounted permanent-magnet machines," *IEEE Access*, vol. 7, pp. 148453–148461, 2019.

[3] I. Takahashi and T. Noguchi, "A new quick-response and high-efficiency control strategy of an induction motor," *IEEE Trans. Ind. Appl.*, vol. IA-22, no. 5, pp. 820–827, Sep. 1986.

[4] U. Baader, M. Depenbrock, and G. Gierse, "Direct self control (DSC) of inverter-fed induction machine: A basis for speed control without speed measurement," *IEEE Trans. Ind. Appl.*, vol. 28, no. 3, pp. 581–588, May/Jun. 1992.

[5] D. Casadei, F. Profumo, G. Serra, and A. Tani, "FOC and DTC: Two viable schemes for induction motors torque control," *IEEE Trans. Power Electron.*, vol. 17, no. 5, pp. 779–787, Sep. 2002.
[6] F. B. Salem, A. Yangui, and A. Masmoudi, "On the reduction of the commutation frequency in DTC: A comparative study," *Eur. Trans. Electr. Power*, vol. 15, no. 6, pp. 571–584, 2005.
[7] D. Rekioua and T. Rekioua, "DSP-controlled direct torque control of induction machines based on modulated hysteresis control," in *Proc. Int. Conf. Microelectron. (ICM)*, Marrakech, Morocco, Dec. 2009, pp. 378–381.
[8] M. Uddin and M. Hafeez, "FLC-based DTC scheme to improve the dynamic performance of an IM drive," *IEEE Trans. Ind. Appl.*, vol. 48, no. 2, pp. 823–831, Mar. 2012.
[9] K. Bouhoune, K. Yazid, and M. S. Boucherit, "ANN-based DTC scheme to improve the dynamic performance of an IM drive," in *Proc. 7th IET Int. Conf. Power Electron., Mach. Drives (PEMD)*, Manchester, U.K., 2014, pp. 1–6.
[10] S. Krim, S. Gdaim, A. Mtibaa, and M. F. Mimouni, "Control with high performances based DTC strategy: FPGA implementation and experimental validation," *EPE J.*, vol. 29, no. 2, pp. 82–98, Apr. 2019.
[11] S. Kouro, M. A. Perez, J. Rodriguez, A. M. Llor, and H. A. Young, "Model predictive control: MPC's role in the evolution of power electronics," *IEEE Ind. Electron. Mag.*, vol. 9, no. 4, pp. 8–21, Dec. 2015.
[12] Y. Zhang and H. Yang, "Two-vector-based model predictive torque control without weighting factors for induction motor drives," *IEEE Trans. Power Electron.*, vol. 31, no. 2, pp. 1381–1390, Feb. 2016.
[13] S. V. Pérez, J. Rodríguez, M. Rivera, L. G. Franquelo, and M. Norambuena, "Model predictive control for power converters and drives: Advances and trends," *IEEE Trans. Ind. Electron.*, vol. 64, no. 2, pp. 935–947, Feb. 2017.
[14] S. Madanzadeh, A. Abedini, A. Radan, and J.-S. Ro, "Application of quadratic linearization state feedback control with hysteresis reference reformer to improve the dynamic response of interior permanent magnet synchronous motors," *ISA Trans.*, vol. 99, pp. 167–190, Apr. 2020.
[15] J. Rodríguez and P. Cortés, *Predictive Control of Power Converters and Electrical Drives*. Hoboken, NJ, USA: Wiley, 2012.
[16] Y. Deng, Z. Liang, P. Xia, and X. Zuo, "Improved speed sensorless vector control algorithm of induction motor based on long cable," *J. Electr. Eng. Technol.*, vol. 14, no. 1, pp. 219–229, Jan. 2019.
[17] S. Singh and A. N. Tiwari, "Various techniques of sensorless speed control of PMSM: A review," in *Proc. 2nd Int. Conf. Electr., Comput. Commun. Technol. (ICECCT)*, Coimbatore, India, Feb. 2017, pp. 1–6.
[18] N. Ali, A. U. Rehman, W. Alam, and H. Maqsood, "Disturbance observer based robust sliding mode control of permanent magnet synchronous motor," *J. Electr. Eng. Technol.*, vol. 14, no. 6, pp. 2531–2538, Nov. 2019.
[19] A. Ammar, A. Bourek, and A. Benakcha, "Sensorless SVM-direct torque control for induction motor drive using sliding mode observers," *J. Control, Autom. Electr. Syst.*, vol. 28, no. 2, pp. 189–202, Apr. 2017.
[20] H. Wang, Y.-C. Liu, and X. Ge, "Sliding-mode observer-based speed-sensorless vector control of linear induction motor with a parallel secondary resistance online identification," *IET Electr. Power Appl.*, vol. 12, no. 8, pp. 1215–1224, Sep. 2018.
[21] H. Kubota and K. Matsuse, "Speed sensorless field-oriented control of induction motor with rotor resistance adaptation," *IEEE Trans. Ind. Appl.*, vol. 30, no. 5, pp. 1219–1224, Sep./Oct. 1994.
[22] Z. Qu, M. Hinkkanen, and L. Harnefors, "Gain scheduling of a full-order observer for sensorless induction motor drives," *IEEE Trans. Ind. Appl.*, vol. 50, no. 6, pp. 3834–3845, Nov. 2014.
[23] B. Chen, T. Wang, Z. Lu, W. Yao, and K. Lee, "Speed convergence rate-based feedback gains design of adaptive full-order observer in sensorless induction motor drives," *IET Electr. Power Appl.*, vol. 8, no. 1, pp. 13–22, Jan. 2014.
[24] A. Derdiyok, "Speed-sensorless control of induction motor using a continuous control approach of sliding-mode and flux observer," *IEEE Trans. Ind. Electron.*, vol. 52, no. 4, pp. 1170–1176, Aug. 2005.
[25] Q. Wang, H. Yu, M. Wang, and X. Qi, "An improved sliding mode control using disturbance torque observer for permanent magnet synchronous motor," *IEEE Access*, vol. 7, pp. 36691–36701, 2019.
[26] Z. Ma and X. Zhang, "FPGA implementation of sensorless sliding mode observer with a novel rotation direction detection for PMSM drives," *IEEE Access*, vol. 6, pp. 55528–55536, 2018.
[27] J. Rodríguez, J. Pontt, C. Silva, P. Cortés, S. Rees, and U. Ammann, "Predictive direct torque control of an induction machine," in *Proc. Power Electron. Motion Control Conf.*, 2004, vol. 2, no. 4.
[28] H. Miránda, P. Cortés, J. I. Yuz, and J. Rodríguez, "Predictive torque control of induction machines based on state-space models," *IEEE Trans. Ind. Electron.*, vol. 56, no. 6, pp. 1916–1924, Jun. 2009.
[29] M. Habibullah, D. D.-C. Lu, D. Xiao, and M. F. Rahman, "Finite-state predictive torque control of induction motor supplied from a three-level NPC voltage source inverter," *IEEE Trans. Power Electron.*, vol. 32, no. 1, pp. 479–489, Jan. 2017.
[30] A. A. Ahmed, B. K. Koh, H. S. Park, K.-B. Lee, and Y. I. Lee, "Finite-control set model predictive control method for torque control of induction motors using a state tracking cost index," *IEEE Trans. Ind. Electron.*, vol. 64, no. 3, pp. 1916–1928, Mar. 2017.
[31] R. K. Munje, M. R. Roda, and B. E. Kushare, "Speed control of DC motor using PI and SMC," in *Proc. IPEC*, Singapore, Oct. 2010, pp. 945–950.
[32] Z. Yongchang and Z. Zhengming, "Comparative study of PI, sliding mode and fuzzy logic controller for rotor field oriented controlled induction motor drives," in *Proc. Int. Conf. Electr. Mach. Syst.*, Wuhan, China, 2008, pp. 1089–1094.
[33] I. Sami, B. Khan, R. Asghar, C. A. Mehmood, S. M. Ali, Z. Ullah, and A. Basit, "Sliding mode-based model predictive torque control of induction machine," in *Proc. Int. Conf. Eng. Emerg. Technol. (ICEET)*, Lahore, Pakistan, Feb. 2019, pp. 1–5.
[34] A. S. Faskhodi and A. Fakharian, "Output feedback robust siding mode controller design for wind turbine," *J. Electr. Eng. Technol.*, vol. 14, no. 6, pp. 2477–2485, Nov. 2019.
[35] S. Krim, S. Gdaim, and M. F. Mimouni, "Robust direct torque control with super-twisting sliding mode control for an induction motor drive," *Complexity*, vol. 2019, pp. 1–24, Jun. 2019.
[36] F. Plestan, Y. Shtessel, V. Brégeault, and A. Poznyak, "New methodologies for adaptive sliding mode control," *Int. J. Control*, vol. 83, no. 9, pp. 1907–1919, Sep. 2010.
[37] Y. Wang, K. Zhu, B. Chen, and M. Jin, "Model-free continuous nonsingular fast terminal sliding mode control for cable-driven manipulators," *ISA Trans.*, vol. 98, pp. 483–495, Mar. 2020.
[38] Y. Wang, S. Li, D. Wang, F. Ju, B. Chen, and H. Wu, "Adaptive time-delay control for cable-driven manipulators with enhanced nonsingular fast terminal sliding mode," *IEEE Trans. Ind. Electron.*, early access, Feb. 26, 2020, doi: 10.1109/TIE.2020.2975473.
[39] Y. Wang, L. Liu, D. Wang, F. Ju, and B. Chen, "Time-delay control using a novel nonlinear adaptive law for accurate trajectory tracking of cable-driven robots," *IEEE Trans. Ind. Informat.*, vol. 16, no. 8, pp. 5234–5243, Aug. 2020.
[40] Y. Wang, F. Yan, J. Chen, F. Ju, and B. Chen, "A new adaptive time-delay control scheme for cable-driven manipulators," *IEEE Trans. Ind. Informat.*, vol. 15, no. 6, pp. 3469–3481, Jun. 2019.
[41] S. Di Gennaro, J. Rivera, and B. Castillo-Toledo, "Super-twisting sensorless control of permanent magnet synchronous motors," in *Proc. 49th IEEE Conf. Decis. Control (CDC)*, Atlanta, GA, USA, Dec. 2010, pp. 4018–4023.
[42] A. Chalanga, S. Kamal, L. M. Fridman, B. Bandyopadhyay, and J. A. Moreno, "Implementation of super-twisting control: Super-twisting and higher order sliding-mode observer-based approaches," *IEEE Trans. Ind. Electron.*, vol. 63, no. 6, pp. 3677–3685, Jun. 2016.
[43] Z. Li, S. Zhou, Y. Xiao, and L. Wang, "Sensorless vector control of permanent magnet synchronous linear motor based on self-adaptive super-twisting sliding mode controller," *IEEE Access*, vol. 7, pp. 44998–45011, 2019.
[44] O. A. Morfin, F. A. Valenzuela, R. R. Betancour, C. E. Castañeda, R. Ruíz-Cruz, and A. Valderrabano-Gonzalez, "Real-time SOSM super-twisting combined with block control for regulating induction motor velocity," *IEEE Access*, vol. 6, pp. 25898–25907, 2018.
[45] C. Evangelista, P. Puleston, and F. Valenciaga, "Wind turbine efficiency optimization. Comparative study of controllers based on second order sliding modes," *Int. J. Hydrogen Energy*, vol. 35, no. 11, pp. 5934–5939, Jun. 2010.
[46] I. Matraji, F. S. Ahmed, S. Laghrouche, and M. Wack, "Comparison of robust and adaptive second order sliding mode control in PEMFC air-feed systems," *Int. J. Hydrogen Energy*, vol. 40, no. 30, pp. 9491–9504, Aug. 2015.
[47] M. Derbeli, M. Farhat, O. Barambones, and L. Sbita, "Control of PEM fuel cell power system using sliding mode and super-twisting algorithms," *Int. J. Hydrogen Energy*, vol. 42, no. 13, pp. 8833–8844, Mar. 2017.

[48] W. C. A. Pereira, C. M. R. Oliveira, M. P. Santana, T. E. P. Almeida, A. G. Castro, G. T. Paula, and M. L. Aguiar, "Improved sensorless vector control of induction motor using sliding mode observer," *IEEE Latin Amer. Trans.*, vol. 14, no. 7, pp. 3110–3116, Jul. 2016.
[49] F. A. Chachar, S. S. H. Bukhari, F. H. Mangi, D. E. Macpherson, G. P. Harrison, W. Bukhsh, and J.-S. Ro, "Hierarchical control implementation for meshed AC/multi-terminal DC grids with offshore windfarms integration," *IEEE Access*, vol. 7, pp. 142233–142245, 2019.
[50] M. M. Zaid and J.-S. Ro, "Switch ladder modified H-bridge multilevel inverter with novel pulse width modulation technique," *IEEE Access*, vol. 7, pp. 102073–102086, 2019.
[51] V. Utkin and J. Shi, "Integral sliding mode in systems operating under uncertainty conditions," in *Proc. 35th IEEE Conf. Decis. Control*, Kobe, Japan, Dec. 1996, pp. 4591–4596.
[52] L. Derafa, A. Benallegue, and L. Fridman, "Super twisting control algorithm for the attitude tracking of a four rotors UAV," *J. Franklin Inst.*, vol. 349, no. 2, pp. 685–699, Mar. 2012.
[53] A. Davila, J. Moreno, and L. Fridman, "Reaching time estimation for super-twisting based on Lyapunov function," in *Proc. IEEE Conf. Decis. Control*, Aug. 2009, pp. 1–7.
[54] M. Labbadi and M. Cherkaoui, "Novel robust super twisting integral sliding mode controller for a quadrotor under external disturbances," *Int. J. Dyn. Control*, vol. 8, pp. 1–11, Dec. 2019.
[55] A. Derdiyok, Z. Yan, M. Guven, and V. Utkin, "A sliding mode speed and rotor time constant observer for induction machines," in *Proc. 27th Annu. Conf. IEEE Ind. Electron. Soc. (IECON)*, Denver, CO, USA, Nov./Dec. 2001, pp. 1400–1405.
[56] K. Ali, S. Ullah, Q. Khan, I. Khan, and L. Khan, "Neurofuzzy robust backstepping based MPPT control for photovoltaic system," *Turkish J. Electr. Eng. Comput. Sci.*, Feb. 2020, doi: 10.3906/elk-1907-15.

IRFAN SAMI received the B.Sc. degree in electrical engineering from the University of Engineering and Technology Peshawar, Bannu Campus, Pakistan, in 2016, and the M.Sc. degree in electrical engineering from COMSATS University Islamabad, Abbottabad Campus, Abbottabad, Pakistan, in 2019. He is currently pursuing the Ph.D. degree in electrical engineering with the Chung-Ang University, Seoul, South Korea. His research interests include electric drives, renewable energies, and electrical machine design.

SHAFAAT ULLAH was born in Lakki Marwat, Khyber Pakhtunkhwa, Pakistan. He received the B.Sc. and M.Sc. degrees in electrical engineering from the University of Engineering and Technology Peshawar, Pakistan, in 2007 and 2013, respectively.

He has served as an Assistant Director of the Pakistan Council of Renewable Energy Technologies (PCRET), and as the Assistant Manager (Operation)/Junior Engineer (Electrical) of the Lahore Electric Supply Company (LESCO), Pakistan.

ABDUL BASIT received the B.Sc. degree in electrical engineering from the University of Engineering and Technology Peshawar, Bannu Campus, Pakistan, in 2015, and the M.Sc. degree in electrical engineering from COMSATS University Islamabad, Abbottabad Campus, Abbottabad, Pakistan, in 2019. His research interests include electric drives control and renewable energy integration in smart grids.

NASIM ULLAH received the Ph.D. degree in mechatronics engineering from Beihang University, Beijing, China, in 2013. From 2006 to 2010, he was a Senior Design Engineer with IICS, Pakistan. He is currently an Associate Professor of Electrical Engineering with Taif University, Saudi Arabia. His research interests include renewable energy, flight control systems, integer and fractional order modeling of dynamic systems, integer/fractional-order adaptive robust control methods, fuzzy/NN, hydraulic and electrical servos, epidemic, and vaccination control strategies.

JONG-SUK RO received the B.S. degree in mechanical engineering from the Han-Yang University, Seoul, South Korea, in 2001, and the Ph.D. degree in electrical engineering from the Seoul National University (SNU), Seoul, in 2008. He is currently pursuing the Ph.D. degree in electrical engineering with the COMSATS University Islamabad, Abbottabad Campus, Abbottabad, Pakistan.

He is an Associate Professor with the School of Electrical and Electronics Engineering, Chung-Ang University, Seoul. In 2014, he was with the University of Bath, Bath, U.K., as an Academic Visitor. From 2013 to 2016, he worked with the Brain Korea 21 Plus, SNU, as a BK Assistant Professor. He conducted research at the Electrical Energy Conversion Systems Research Division of the Korea Electrical Engineering and Science Research Institute as a Researcher, in 2013. From 2012 to 2013, he was with the Brain Korea 21 Information Technology, SNU, as a Postdoctoral Fellow. He conducted research at the Research and Development Center, Samsung Electronics, as a Senior Engineer, from 2008 to 2012. He is also serving as an Assistant Professor (on Ph.D. Study Leave) with the Department of Electrical Engineering, University of Engineering and Technology Peshawar, Bannu Campus, Bannu, Pakistan. His research interests include the analysis and optimal design of next-generation electrical machines using smart materials, such as electromagnets, piezoelectric, and magnetic shape memory alloys, as well as photovoltaics, wind energy conversion systems, and distributed control of multi-agent-based smart grids.